

Microscopic Understanding of Ultrafast Charge Transfer in van der Waals Heterostructures

R. Krause^{1,2,*}, S. Aeschlimann^{1,2}, M. Chávez-Cervantes,² R. Perea-Causin,³ S. Brem,⁴ E. Malic,^{4,3} S. Forti,⁵ F. Fabbri^{5,6,7}, C. Coletti,^{5,7} and I. Gierz^{1,†}

¹University of Regensburg, Institute for Experimental and Applied Physics, 93040 Regensburg, Germany

²Max Planck Institute for the Structure and Dynamics of Matter, Center for Free Electron Laser Science, 22761 Hamburg, Germany


³Chalmers University of Technology, Department of Physics, 41296 Gothenburg, Sweden

⁴Philipps-Universität Marburg, Department of Physics, 35032 Marburg, Germany

⁵Center for Nanotechnology Innovation at NEST, Istituto Italiano di Tecnologia, 56127 Pisa, Italy

⁶NEST, Istituto Nanoscienze, CNR and Scuola Normale Superiore, 56127 Pisa, Italy

⁷Graphene Labs, Istituto Italiano di Tecnologia, 16163 Genova, Italy

 (Received 3 May 2021; revised 29 September 2021; accepted 12 November 2021; published 27 December 2021)

Van der Waals heterostructures show many intriguing phenomena including ultrafast charge separation following strong excitonic absorption in the visible spectral range. However, despite the enormous potential for future applications in the field of optoelectronics, the underlying microscopic mechanism remains controversial. Here we use time- and angle-resolved photoemission spectroscopy combined with microscopic many-particle theory to reveal the relevant microscopic charge transfer channels in epitaxial WS₂/graphene heterostructures. We find that the timescale for efficient ultrafast charge separation in the material is determined by direct tunneling at those points in the Brillouin zone where WS₂ and graphene bands cross, while the lifetime of the charge separated transient state is set by defect-assisted tunneling through localized sulphur vacancies. The subtle interplay of intrinsic and defect-related charge transfer channels revealed in the present work can be exploited for the design of highly efficient light harvesting and detecting devices.

DOI: [10.1103/PhysRevLett.127.276401](https://doi.org/10.1103/PhysRevLett.127.276401)

Stacking different two-dimensional materials in a lego-like manner enables the formation of novel ultimately thin heterostructures with tailored electronic properties exploiting screening and proximity-induced effects [1–3]. These van der Waals (vdW) heterostructures exhibit many intriguing phenomena including ultrafast charge separation following optical excitation [4] and bear great promise for future applications in the field of optoelectronics [5]. Among the huge variety of existing vdW heterostructures those that combine monolayer graphene with a monolayer of one of the semiconducting transition metal dichalcogenides (TMDs) are of particular interest [6]. These heterostructures exhibit type I band alignment where both the minimum of the conduction band (CBM) and the maximum of the valence band (VBM) are located in the graphene layer. Strong excitonic absorption in the TMD monolayer is then followed by ultrafast charge transfer into the graphene layer [7–13]. Previous studies on WS₂/graphene heterostructures have shown that hole transfer is considerably faster than electron transfer, resulting in a charge-separated transient state [14,15]. Despite the enormous potential for future applications in the field of optoelectronics and optospintronics, the microscopic mechanism underlying the ultrafast charge transfer processes in TMD/graphene and similar heterostructures remains poorly understood.

In this work we tackle this problem with a combination of time- and angle-resolved photoemission spectroscopy (tr-ARPES) [14] and microscopic many-particle theory [16–18]. We resonantly excite the A exciton in epitaxial WS₂/graphene heterostructures [19,20] and find that both electron and hole transfer become faster with increasing pump fluence. We explain this with the help of a tunneling model where hot carriers transfer from WS₂ to graphene at those points in momentum space where the respective bands cross. We also find that the lifetime of the charge separated state increases with increasing fluence, indicating the importance of S vacancies [21–23] that efficiently trap photoexcited electrons in the WS₂ layer [15]. The microscopic insights gained in the present study will guide the design of future optoelectronic and optospintronic devices where defects and band alignment will serve as important control parameters.

WS₂/graphene heterostructures were grown on H-terminated SiC(0001) as described in Refs. [19,20,24,25]. 2 eV pump and 26 eV probe pulses for the tr-ARPES experiments were generated by frequency doubling the signal output of an optical parametric amplifier and by high harmonics generation in argon, respectively. The tunneling matrix elements for electrons and holes were computed using microscopic many-particle theory [16–18,26–30].

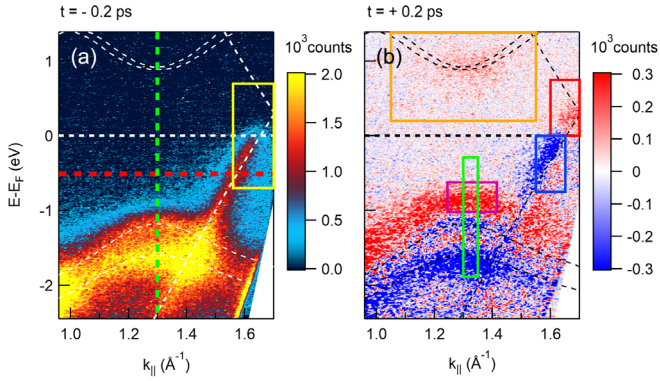


FIG. 1. Tr-ARPES snapshots of WS₂/graphene heterostructure before and after optical excitation. (a) Photocurrent measured along the ΓK direction at negative pump-probe delay. Colored dashed lines indicate the position of the line profiles used to determine the transient band positions in Figs. 2(c) and 2(e). The yellow box indicates the region where the Fermi-Dirac fits for Fig. 4(b) were performed. (b) Pump-induced changes of the photocurrent at the peak of the pump-probe signal. Red and blue indicate gain and loss of photoelectrons, respectively, with respect to the photocurrent measured at negative pump-probe delay. Colored boxes indicate the areas of integration for the pump-probe traces shown in Figs. 2(a) and 2(b). Thin dashed lines represent the calculated band structures of graphene [32] and WS₂ [33]. Rigid band shifts of -0.81 eV and -1.19 eV were applied to WS₂ CB and VB, respectively. The graphene Dirac cone was shifted by $+0.3$ eV to account for the observed hole doping [25].

Further details about the various methods employed in the present study are given in the Supplemental Material [31].

In Fig. 1 we show tr-ARPES snapshots measured along the ΓK direction of the hexagonal Brillouin zone close to the graphene and WS₂ K points for different pump-probe delays after photoexcitation at $\hbar\omega_{\text{pump}} = 2$ eV with a pump fluence of 2.85 mJ/cm². Within our experimental resolution (170 meV in this particular dataset) the unperturbed band structure measured at negative pump-probe delay [Fig. 1(a)] is well described by the sum of the calculated band structures of the individual layers [32,33] (thin white dashed lines) after applying rigid band shifts to account for doping and to reproduce the experimentally observed WS₂ band gap. At the peak of the pump-probe signal [Fig. 1(b)] we observe a gain of photoelectrons at the bottom of the WS₂ conduction band (CB), a strong gain-and-loss signal for the WS₂ valence band (VB), and a strong gain-and-loss signal for the graphene Dirac cone. We interpret these features in terms of electron-hole pair generation followed by ultrafast charge separation as discussed in detail below [14].

For further analysis we present momentum-resolved population dynamics [Figs. 2(a) and 2(b)] as well as transient peak positions of the individual electronic bands [Figs. 2(c) and 2(d)] that serve as smoking gun evidence for ultrafast charge separation in the system. The data points in

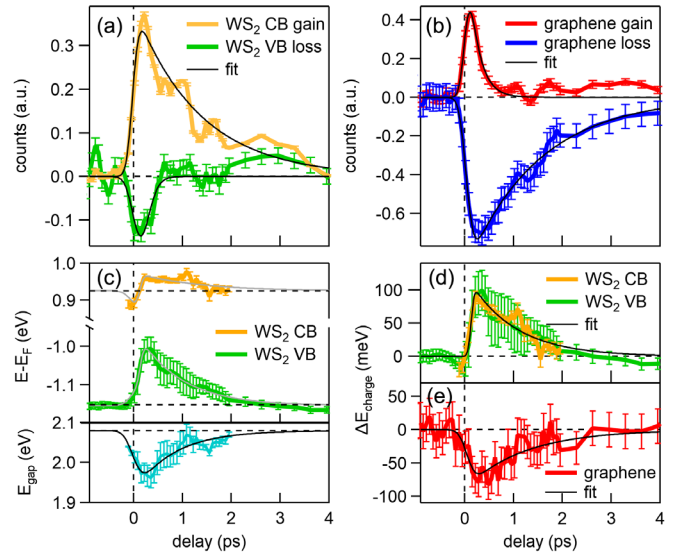


FIG. 2. Evidence for ultrafast charge separation: (a) Gain in the WS₂ CB (orange) and loss in the WS₂ VB (green). (b) Gain above the Fermi level (red) and loss below the Fermi level (blue) inside the graphene Dirac cone. (c) Position of the WS₂ CB (orange) and the upper WS₂ VB (green) and transient band gap of WS₂ (turquoise). (d) Charging-induced shift of WS₂ valence and conduction band. (e) Transient shift of the graphene Dirac cone. All quantities are plotted as a function of pump-probe delay. Black lines are single exponential fits to the data. Gray lines in panel (c) were calculated from the exponential fit for E_{gap} in panel (c) and the exponential fit in panel (d).

Figs. 2(a) and 2(b) were obtained by integrating the photocurrent over the areas indicated by the colored boxes in Fig. 1(b). They show the population dynamics of the WS₂ valence and conduction band [Fig. 2(a)] and the graphene Dirac cone [Fig. 2(b)] as a function of pump-probe delay. Thin black lines are single exponential fits to the data [31]. We find that gain and loss traces for both WS₂ and graphene are asymmetric. The WS₂ valence and conduction band shows a short-lived loss ($\tau = 100 \pm 40$ fs) and long-lived gain ($\tau = 1.3 \pm 0.1$ ps), respectively. The situation is reversed in the graphene layer where the gain above the Fermi level is found to be short-lived ($\tau = 210 \pm 20$ fs) and the loss below the Fermi level is found to be long-lived ($\tau = 1.50 \pm 0.06$ ps). This behavior is not observed in individual graphene and WS₂ layers and indicates ultrafast charge separation [14]. In detail, the short lifetime of the loss in the WS₂ VB and the gain above the Fermi level in the graphene Dirac cone indicate that the photoexcited holes in the WS₂ layer are rapidly (on a timescale comparable to the temporal resolution of 200 fs) refilled by electrons from graphene. The photoexcited electrons, on the other hand, are found to remain in the WS₂ CB for $\tau = 1.3 \pm 0.1$ ps.

The resulting charge separated transient state leaves the WS₂ layer negatively charged and the graphene layer positively charged. This is expected to decrease the binding

energy of the WS₂ states and increase the binding energy of the graphene states [14]. In Fig. 2(c) we plot the transient peak positions of the upper WS₂ VB and the WS₂ CB that were obtained by fitting energy distribution curves (EDCs) through the *K* point of WS₂ [dashed green line in Fig. 1(a)] with a Gaussian [31]. The energy difference between the WS₂ CB and VB directly yields the transient band gap E_{gap} shown in the lower part of Fig. 2(c). From an exponential fit to the data [31] we deduce an equilibrium gap size of 2.08 eV and a lifetime of $\tau = 0.8 \pm 0.4$ ps for the transient band gap renormalization ΔE_{gap} . The renormalization is a consequence of increased screening in the presence of photoexcited carriers and is commonly observed in photo-doped TMD monolayers [34–37]. Assuming that band gap renormalization shifts the WS₂ VB up and the WS₂ CB down by the same amount $|\Delta E_{\text{gap}}|/2$ we can subtract its contribution from the transient peak positions in Fig. 2(c) yielding the data in Fig. 2(d) where both the WS₂ valence and conduction band are found to shift up by ~ 100 meV with a lifetime of $\tau = 1.03 \pm 0.07$ ps. This shift is attributed to the transient negative charging of the WS₂ layer. The transient position of graphene’s Dirac cone in Fig. 2(e) was extracted from Lorentzian fits of momentum distribution curves (MDCs) [31] at $E = -0.5$ eV extracted along the dashed red line in Fig. 1(a). The resulting momentum shift was converted into an energy shift by multiplying with the slope of the band $\nu_F = 7$ eV Å [38]. The observed increase in binding energy with an exponential lifetime of 1.08 ± 0.06 ps is a direct consequence of the additional positive charge on the graphene layer due to ultrafast hole transfer.

In order to gain access to the microscopic mechanism underlying the observed ultrafast charge transfer phenomena we now investigate the pump fluence dependence of the electron and hole transfer rates as well as the lifetime of the charge separated state. As discussed above, the short-lived loss in the WS₂ VB [Fig. 2(a)] is directly linked to the short-lived gain above the Fermi level in the Dirac cone of graphene [Fig. 2(b)]. The signal-to-noise ratio, however, is much better in the latter case, which is why we focus on the graphene gain rather than the WS₂ VB loss to analyze the pump fluence dependence of the ultrafast hole transfer. The result is shown in Fig. 3(a). We find that the hole transfer time of ~ 1 ps observed at the lowest pump fluence rapidly drops to a value short compared to our temporal resolution of 200 fs with increasing fluence. Figure 3(b) shows the pump fluence dependence of the lifetime of the photoexcited electrons in the conduction band of WS₂ from Fig. 2(a). This value is found to decrease from ~ 2 ps at the lowest fluence to below 1 ps at the highest fluence. In Fig. 3(c) we plot the pump fluence dependence of the gain above the equilibrium position of the upper WS₂ VB obtained by integrating the photocurrent over the area indicated by the pink box in Fig. 1(b). We confirmed that this quantity shows the same fluence dependence as the

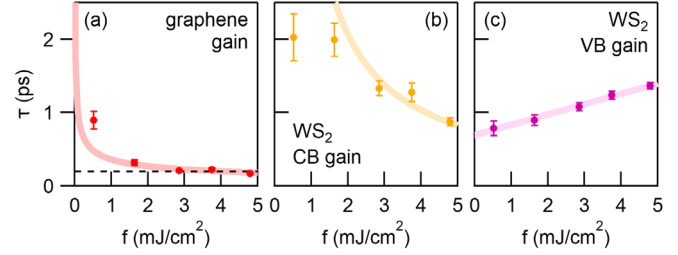


FIG. 3. Fluence dependence of ultrafast charge separation and recombination: (a) Lifetime of graphene gain from Fig. 2(b). The black dashed line represents our temporal resolution of 200 fs. (b) Lifetime of photoexcited electrons in the WS₂ CB from Fig. 2(a). (c) Lifetime of gain above the equilibrium position of the upper WS₂ VB. Thick lines in (a) and (b) were obtained by inverting and rescaling the guides to the eye from Fig. 4(d) to match the data points. The thick line in (c) is a guide to the eye.

charging-induced band shifts in Figs. 2(d) and 2(e) [31] albeit with an improved signal-to-noise ratio. From Fig. 3(c) we find that the lifetime of the charge separated state linearly increases with increasing fluence from ~ 0.8 ps at the lowest fluence to ~ 1.4 ps at the highest fluence. In summary, Fig. 3 shows that the transfer rate of the holes increases with increasing fluence, the lifetime of the photoexcited electrons in the CB of WS₂ decreases with increasing fluence, and the lifetime of the charge separated state increases with increasing fluence.

A detailed comparison with related experimental and theoretical work [13,36,39–41] is given in [31]. In a nutshell, Refs. [13,36] investigated similar type I heterostructures made of either MoS₂ or WS₂ and graphene. In contrast to the present study, Ref. [36] found no indication for charge separation which is likely due to the twist angle of 30° between MoS₂ and graphene that changes the location of the crossing points of the bands in the Brillouin zone. Reference [13] observed no systematic pump fluence dependence of the relaxation times in WS₂/graphene heterostructures with unknown twist angle. Their model, where the electric field across the interface that builds up due to charge separation increases the transfer rate for the electrons, can be reconciled with our observation in Fig. 3(b). However, this model cannot explain our observation that the hole transfer rate also increases with increasing fluence [see Fig. 3(a)]. Finally, Refs. [39–41] proposed a coherent phonon-driven charge transfer mechanism for ultrafast charge separation in type II heterostructures that cannot be directly applied to our WS₂/graphene heterostructure with type I band alignment. Therefore, we evoke a new scenario where carriers can tunnel from one layer to the other at the points in momentum space where the bands of the individual layers cross and where charge transfer can occur without energy or momentum transfer. In this scenario the transfer rate is proportional to $e^{-\Delta E/k_B T}$, where the energy barrier ΔE is given by the distance between the WS₂ VBM or CBM and

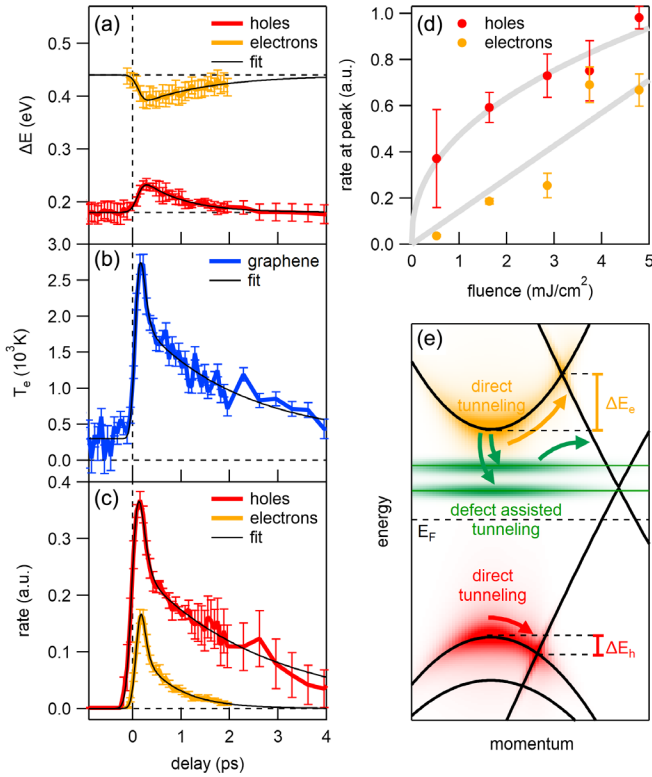


FIG. 4. Direct tunneling model. (a) Temporal evolution of the two barrier heights deduced from Fig. 2 together with single-exponential fit. (b) Temporal evolution of the electronic temperature inside the Dirac cone together with double-exponential fit. (c) Temporal evolution of the electron and hole transfer rates deduced from panels (b) and (c) together with double-exponential fit. (d) Pump fluence dependence of the peak transfer rates for electrons and holes determined from exponential fits to the data in Fig. 4(c) [31]. Thick gray lines are guides to the eye. (e) Sketch of the band structure with tunneling barrier for holes (ΔE_h , red) and electrons (ΔE_e , orange). Our final microscopic model includes direct (orange and red arrows) as well as defect-assisted tunneling (green arrows).

the closest crossing point [Fig. 4(e)] and where $k_B T$ is the thermal energy of the carriers. The temporal evolution of the energy barriers for electron and hole transfer [Fig. 4(a)] was deduced from the transient band shifts in Fig. 2. The temperature of the electron-hole pairs in WS_2 is difficult to determine experimentally due to the short lifetime of the holes and the limited signal-to-noise ratio. The electronic temperature of the Dirac carriers inside the graphene layer [Fig. 4(b)] on the other hand can be easily extracted from Fermi-Dirac fits of the transient carrier distribution inside the Dirac cone as described in [31]. Assuming that the electronic temperature for the carriers inside the Dirac cone is similar to the one of the carriers in the WS_2 layer [31], we can determine the temporal evolution of the transfer rates shown in Fig. 4(c). The peak rate is found to be faster for holes than for electrons and to increase with increasing fluence for both electrons and holes [Fig. 4(d)] in good qualitative agreement with the data in Fig. 3.

To confirm the above interpretation, we calculated the transfer times for electrons and holes using a microscopic model based on the density matrix formalism [16–18,42], which is further described in [31]. The momentum dependence of the tunneling matrix element evaluated on a tight-binding level for the CB and VB is shown in Figs. 5(a) and 5(b), respectively, together with black lines that indicate the position in momentum space where the crossing between the WS_2 CB and VB, respectively, and the Dirac cone occurs. The tunneling matrix elements exhibit a strong momentum dependence that can be traced back to the pseudospin of the Dirac carriers in the graphene layer that has opposite helicity for VB and CB [38]. More importantly, the tunneling matrix element in the region of interest indicated by the black lines in Figs. 5(a) and 5(b) is found to be much bigger for the VB than for the CB. In addition to the different energy barriers found in Fig. 4(a) this accounts for the experimentally observed asymmetry between electron and hole transfer. We also calculated the transfer times for holes and electrons as a function of the height of the respective energy barrier and the carrier temperature in Figs. 5(c) and 5(d). In good qualitative agreement with our experiment, the calculated lifetimes are found to decrease with increasing carrier temperature (i.e., with increasing pump fluence), while the change in barrier height (< 100 meV in the experiment) is found to have a minor influence on the fluence dependence of the lifetimes.

While this model nicely explains the observed fluence dependence of the carrier lifetimes in Figs. 3(a) and 3(b), it fails to reproduce the fact that the lifetime of the charge separated transient state is found to increase with increasing fluence [Fig. 3(c)]. This indicates that, in addition to the direct tunneling scenario proposed above, there are additional charge transfer channels that need to be considered for a full microscopic understanding of the ultrafast charge transfer processes in our WS_2 /graphene heterostructure. A likely candidate are defect-related charge transfer channels involving S vacancies [22,23]. It has been shown using scanning tunneling spectroscopy combined with GW calculations [23] that S vacancies give rise to two spin-orbit split states inside the band gap of WS_2 that also appear in our tr-ARPES data (see Fig. 11 in [31]). These states were proposed to efficiently trap photoexcited electrons inside the WS_2 layer and thereby enhance the lifetime of the charge separated state [15].

In Fig. 4(e) we summarize our understanding of the relevant microscopic scattering channels that mediate the ultrafast charge transfer in our WS_2 /graphene heterostructure. Direct tunneling (orange and red arrows) sets the timescale for charge separation, while defect-assisted tunneling (green arrows) sets the timescale for charge recombination. This model resolves two important controversies in literature. First, it remains unresolved whether charge transfer occurs at Γ , Σ , or K [28,39–41,43,44]. Our findings suggest that ultrafast charge transfer in the

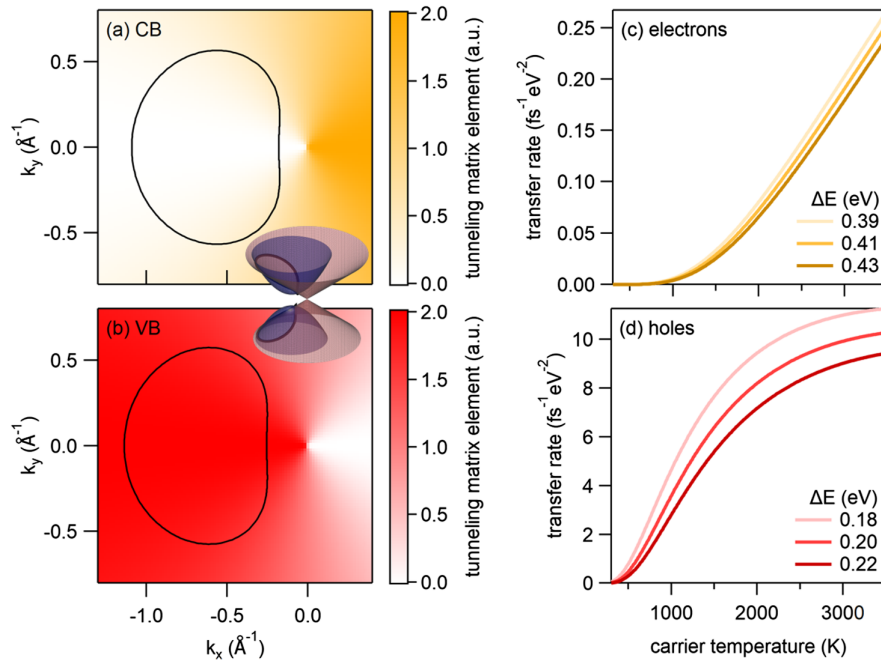


FIG. 5. Microscopic theory. Momentum dependence of the tunneling matrix element for the CB (a) and VB (b). $k_x = k_y = 0$ corresponds to the K point of graphene. Black lines indicate the location of the intersection between WS_2 and graphene bands as illustrated in the inset. Calculated transfer rate for electrons (c) and holes (d) as a function of carrier temperature for different barrier heights.

investigated epitaxial WS_2 /graphene heterostructure occurs at the band intersections close to the K point. The second unresolved issue is related to momentum conservation during charge transfer [28,45]. We propose that ultrafast charge separation occurs via direct tunneling with zero momentum transfer. Charge carrier recombination is dominated by defect-assisted tunneling where the strong localization of the defect states in real space leads to a delocalization over a big part of the Brillouin zone which again enables tunneling at zero momentum transfer.

In summary we combined tr-ARPES with microscopic many-particle theory to unravel the microscopic mechanism of ultrafast charge separation and recombination in epitaxial WS_2 /graphene heterostructures. We find a subtle interplay between direct tunneling at the band intersections close to the K point that sets the timescale for charge separation and defect-assisted tunneling via localized S vacancies that sets the timescale for electron-hole recombination. Our findings will guide the development of improved optoelectronic devices where defect and band structure engineering will serve as important control parameters.

We thank S. Latini, L. Xian, A. Rubio, and S. Refaely-Abramson for many fruitful discussions. This work was supported by the Deutsche Forschungsgemeinschaft through SFB 925, SFB 1083 and SFB 1277, by the European Unions Horizon 2020 research and innovation program under Grant Agreements No. 785219 and

No. 881603, and by the Swedish Research Council (VR, Project No. 2018-00734). The computations were enabled by resources provided by the Swedish National Infrastructure for Computing (SNIC) at C3SE partially funded by the Swedish Research Council through Grant Agreement No. 2016-07213. R. P. C. acknowledges funding from the Excellence Initiative Nano (Chalmers) under the Excellence Ph.D. programme.

*razvan.krause@ur.de

†isabella.gierz@ur.de

- [1] A. K. Geim and I. V. Grigorieva, Van der Waals heterostructures, *Nature (London)* **499**, 419 (2013).
- [2] K. S. Novoselov, A. Mishchenko, A. Carvalho, and A. H. C. Neto, 2D materials and van der Waals heterostructures, *Science* **353**, aac9439 (2016).
- [3] P. Merkl, F. Mooshammer, P. Steinleitner, A. Girmhuber, K.-Q. Lin, P. Nagler, J. Holler, C. Schller, J. M. Lupton, T. Korn, S. Ovesen, S. Brem, E. Malic, and R. Huber, Ultrafast transition between exciton phases in van der Waals heterostructures, *Nat. Mater.* **18**, 691 (2019).
- [4] C. Jin, E. Y. Ma, O. Karni, E. C. Regan, F. Wang, and T. F. Heinz, Ultrafast dynamics in van der Waals heterostructures, *Nat. Nanotechnol.* **13**, 994 (2018).
- [5] Y. Liu, N. O. Weiss, X. Duan, H.-C. Cheng, Y. Huang, and X. Duan, Van der Waals heterostructures and devices, *Nat. Rev. Mater.* **1**, 16042 (2016).
- [6] E. Lorchat, L. E. P. López, C. Robert, D. Lagarde, G. Froehlicher, T. Taniguchi, K. Watanabe, X. Marie, and

- S. Berciaud, Filtering the photoluminescence spectra of atomically thin semiconductors with graphene, *Nat. Nanotechnol.* **15**, 283 (2020).
- [7] J. He, N. Kumar, M. Z. Bellus, H.-Y. Chiu, D. He, Y. Wang, and H. Zhao, Electron transfer and coupling in graphenestungsten disulfide van der Waals heterostructures, *Nat. Commun.* **5**, 5622 (2014).
- [8] N. Huo, Z. Wei, X. Meng, J. Kang, F. Wu, S.-S. Li, S.-H. Wei, and J. Li, Interlayer coupling and optoelectronic properties of ultrathin two-dimensional heterostructures based on graphene, MoS₂ and WS₂, *J. Mater. Chem. C* **3**, 5467 (2015).
- [9] M. Massicotte, P. Schmidt, F. Violla, K. G. Schdler, A. Reserbat-Plantey, K. Watanabe, T. Taniguchi, K. J. Tielrooij, and F. H. L. Koppens, Picosecond photoresponse in van der Waals heterostructures, *Nat. Nanotechnol.* **11**, 42 (2016).
- [10] H. M. Hill, A. F. Rigosi, A. Raja, A. Chernikov, C. Roquelet, and T. F. Heinz, Exciton broadening in WS₂/graphene heterostructures, *Phys. Rev. B* **96**, 205401 (2017).
- [11] L. Yuan, T.-F. Chung, A. Kuc, Y. Wan, Y. Xu, Y. P. Chen, T. Heine, and L. Huang, Photocarrier generation from interlayer charge-transfer transitions in WS₂-graphene heterostructures, *Sci. Adv.* **4**, e1700324 (2018).
- [12] J. He, D. He, Y. Wang, and H. Zhao, Probing effect of electric field on photocarrier transfer in graphene-WS₂ van der Waals heterostructures, *Opt. Express* **25**, 1949 (2017).
- [13] Z. Song, H. Zhu, W. Shi, D. Sun, and S. Ruan, Ultrafast charge transfer in graphene-WS₂ van der Waals heterostructures, *Optik (Stuttgart)* **174**, 62 (2018).
- [14] S. Aeschlimann, A. Rossi, M. Chávez-Cervantes, R. Krause, B. Arnoldi, B. Stadtmüller, M. Aeschlimann, S. Forti, F. Fabbri, C. Coletti, and I. Gierz-Pehla, Direct evidence for efficient ultrafast charge separation in epitaxial WS₂/graphene heterostructures, *Sci. Adv.* **6**, eaay0761 (2020).
- [15] S. Fu, I. d. Fossé, X. Jia, J. Xu, X. Yu, H. Zhang, W. Zheng, S. Krasel, Z. Chen, Z. M. Wang, K.-J. Tielrooij, M. Bonn, A. J. Houtepen, and H. I. Wang, Long-lived charge separation following pump-energy dependent ultrafast charge transfer in graphene/WS₂ heterostructures, *arXiv:2007.08932*.
- [16] E. Malic and A. Knorr, *Graphene and Carbon Nanotubes: Ultrafast Optics and Relaxation Dynamics* (John Wiley & Sons, New York, 2013).
- [17] S. Brem, C. Linderlv, P. Erhart, and E. Malic, Tunable phases of moiré excitons in van der Waals heterostructures, *Nano Lett.* **20**, 8534 (2020).
- [18] S. Brem, K.-Q. Lin, R. Gillen, J. M. Bauer, J. Maultzsch, J. M. Lupton, and E. Malic, Hybridized intervalley moiré excitons and flat bands in twisted WSe₂ bilayers, *Nanoscale* **12**, 11088 (2020).
- [19] S. Forti, A. Rossi, H. Bch, T. Cavallucci, F. Bisio, A. Sala, T. O. Menteş, A. Locatelli, M. Magnozzi, M. Canepa, K. Mller, S. Link, U. Starke, V. Tozzini, and C. Coletti, Electronic properties of single-layer tungsten disulfide on epitaxial graphene on silicon carbide, *Nanoscale* **9**, 16412 (2017).
- [20] F. Fabbri, F. Dinelli, S. Forti, L. Sementa, S. Pace, G. Piccinini, A. Fortunelli, C. Coletti, and P. Pingue, Edge defects promoted oxidation of monolayer WS₂ synthesized on epitaxial graphene, *J. Phys. Chem. C* **124**, 9035 (2020).
- [21] J.-W. Wei, Z.-W. Ma, H. Zeng, Z.-Y. Wang, Q. Wei, and P. Peng, Electronic and optical properties of vacancy-doped WS₂ monolayers, *AIP Adv.* **2**, 042141 (2012).
- [22] V. Carozo, Y. Wang, K. Fujisawa, B. R. Carvalho, A. McCreary, S. Feng, Z. Lin, C. Zhou, N. Perea-López, A. L. Elías, B. Kabius, V. H. Crespi, and M. Terrones, Optical identification of sulfur vacancies: Bound excitons at the edges of monolayer tungsten disulfide, *Sci. Adv.* **3**, e1602813 (2017).
- [23] B. Schuler, D. Y. Qiu, S. Refaely-Abramson, C. Kastl, C. T. Chen, S. Barja, R. J. Koch, D. F. Ogletree, S. Aloni, A. M. Schwartzberg, J. B. Neaton, S. G. Louie, and A. Weber-Bargioni, Large Spin-Orbit Splitting of Deep In-Gap Defect States of Engineered Sulfur Vacancies in Monolayer WS₂, *Phys. Rev. Lett.* **123**, 076801 (2019).
- [24] K. V. Emtsev, A. Bostwick, K. Horn, J. Jobst, G. L. Kellogg, L. Ley, J. L. McChesney, T. Ohta, S. A. Reshanov, J. Rhrl, E. Rotenberg, A. K. Schmid, D. Waldmann, H. B. Weber, and T. Seyller, Towards wafer-size graphene layers by atmospheric pressure graphitization of silicon carbide, *Nat. Mater.* **8**, 203 (2009).
- [25] C. Riedl, C. Coletti, T. Iwasaki, A. A. Zakharov, and U. Starke, Quasi-Free-Standing Epitaxial Graphene on SiC Obtained by Hydrogen Intercalation, *Phys. Rev. Lett.* **103**, 246804 (2009).
- [26] M. Selig, E. Malic, K. J. Ahn, N. Koch, and A. Knorr, Theory of optically induced Förster coupling in van der Waals coupled heterostructures, *Phys. Rev. B* **99**, 035420 (2019).
- [27] A. Kormányos, G. Burkard, M. Gmitra, J. Fabian, V. Zólyomi, N. D. Drummond, and V. Fal'ko, *k* · *p* theory for two-dimensional transition metal dichalcogenide semiconductors, *2D Mater.* **2**, 022001 (2015).
- [28] Y. Wang, Z. Wang, W. Yao, G.-B. Liu, and H. Yu, Interlayer coupling in commensurate and incommensurate bilayer structures of transition-metal dichalcogenides, *Phys. Rev. B* **95**, 115429 (2017).
- [29] E. Malic, T. Winzer, E. Bobkin, and A. Knorr, Microscopic theory of absorption and ultrafast many-particle kinetics in graphene, *Phys. Rev. B* **84**, 205406 (2011).
- [30] M. Kira and S. W. Koch, Many-body correlations and excitonic effects in semiconductor spectroscopy, *Prog. Quantum Electron.* **30**, 155 (2006).
- [31] See Supplemental Material at <http://link.aps.org/supplemental/10.1103/PhysRevLett.127.276401> for additional details on sample growth and characterization, tr-ARPES experimental setup and data analysis, a detailed comparison with literature and the microscopic model of charge transfer.
- [32] P. R. Wallace, The band theory of graphite, *Phys. Rev.* **71**, 622 (1947).
- [33] H. Zeng, G.-B. Liu, J. Dai, Y. Yan, B. Zhu, R. He, L. Xie, S. Xu, X. Chen, W. Yao, and X. Cui, Optical signature of symmetry variations and spin-valley coupling in atomically thin tungsten dichalcogenides, *Sci. Rep.* **3**, 1608 (2013).
- [34] M. M. Ugeda, A. J. Bradley, S.-F. Shi, F. H. da Jornada, Y. Zhang, D. Y. Qiu, W. Ruan, S.-K. Mo, Z. Hussain, Z.-X. Shen, F. Wang, S. G. Louie, and M. F. Crommie, Giant

- bandgap renormalization and excitonic effects in a monolayer transition metal dichalcogenide semiconductor, *Nat. Mater.* **13**, 1091 (2014).
- [35] A. Chernikov, C. Ruppert, H. M. Hill, A. F. Rigosi, and T. F. Heinz, Population inversion and giant bandgap renormalization in atomically thin WS_2 layers, *Nat. Photonics* **9**, 466 (2015).
- [36] S. Ulstrup, A. G. Cabo, J. A. Miwa, J. M. Riley, S. S. Grønborg, J. C. Johannsen, C. Cacho, O. Alexander, R. T. Chapman, E. Springate, M. Bianchi, M. Dendzik, J. V. Lauritsen, P. D. C. King, and P. Hofmann, Ultrafast band structure control of a two-dimensional heterostructure, *ACS Nano* **10**, 6315 (2016).
- [37] F. Liu, M. E. Ziffer, K. R. Hansen, J. Wang, and X. Zhu, Direct Determination of Band-Gap Renormalization in the Photoexcited Monolayer MoS_2 , *Phys. Rev. Lett.* **122**, 246803 (2019).
- [38] A. H. Castro Neto, F. Guinea, N. M. R. Peres, K. S. Novoselov, and A. K. Geim, The electronic properties of graphene, *Rev. Mod. Phys.* **81**, 109 (2009).
- [39] R. Long and O. V. Prezhdo, Quantum coherence facilitates efficient charge separation at a $MoS_2/MoSe_2$ van der Waals junction, *Nano Lett.* **16**, 1996 (2016).
- [40] H. Wang, J. Bang, Y. Sun, L. Liang, D. West, V. Meunier, and S. Zhang, The role of collective motion in the ultrafast charge transfer in van der Waals heterostructures, *Nat. Commun.* **7**, 11504 (2016).
- [41] Q. Zheng, W. A. Saidi, Y. Xie, Z. Lan, O. V. Prezhdo, H. Petek, and J. Zhao, Phonon-assisted ultrafast charge transfer at van der Waals heterostructure interface, *Nano Lett.* **17**, 6435 (2017).
- [42] S. Ovesen, S. Brem, C. Linderålv, M. Kuisma, T. Korn, P. Erhart, M. Selig, and E. Malic, Interlayer exciton dynamics in van der Waals heterostructures, *Commun. Phys.* **2**, 23 (2019).
- [43] J. Zhang, H. Hong, C. Lian, W. Ma, X. Xu, X. Zhou, H. Fu, K. Liu, and S. Meng, Interlayer-state-coupling dependent ultrafast charge transfer in MoS_2/WS_2 bilayers, *Adv. Sci.* **4**, 1700086 (2017).
- [44] L. Li, R. Long, and O. V. Prezhdo, Charge separation and recombination in two-dimensional MoS_2/WS_2 : Time-domain *ab initio* modeling, *Chem. Mater.* **29**, 2466 (2017).
- [45] X. Zhu, N. R. Monahan, Z. Gong, H. Zhu, K. W. Williams, and C. A. Nelson, Charge transfer excitons at van der Waals interfaces, *J. Am. Chem. Soc.* **137**, 8313 (2015).